A NEW SHOCK-TUBE FACILITY FOR THE STUDY OF HIGH-TEMPERATURE CHEMICAL KINETICS

A Thesis

by

JOSE EMILIANO VIVANCO

Submitted to the Office of Graduate and Professional Studies of
Texas A&M University
in partial fulfillment of the requirements for the degree of

MASTER OF SCIENCE

Chair of Committee,	Eric L. Petersen
Committee Members,	Simon W. North
	David A. Staack
Head of Department,	Andreas Polycarpou

December 2014

Major Subject: Mechanical Engineering

ABSTRACT

A new stainless steel shock-tube facility designed for the study of chemical kinetics at elevated temperatures and pressures is described. It consists of a single-pulse shock tube capable of using both lexan diaphragms and die-scored aluminum disks of up to 4 mm thickness, and it has a relatively large driven-section inner diameter of 16.2 cm to minimize non-ideal boundary layer effects. Test times around 3 milliseconds are achievable at conditions ranging from temperatures between 600 and 4000 K and pressures between 1 and 100 atm behind the reflected shock wave. The facility includes a high-vacuum system capable of achieving ultimate pressures on the order of $1x10^{-6}$ torr, a new gas-delivery system, a shock velocity-measurement scheme, a computer-based data acquisition system, and the option of implementing several optical diagnostics such as absorption and emission spectroscopy. The characterization of the shock tube, which includes pressure behavior, turnaround times and vacuum integrity, are presented. The uncertainty of the experimental temperature behind the reflected shock wave was found to be at most 10 K based on the shock velocity measurement technique used. A validation study for the facility was performed using methane-air as well as fuel-O_2 mixtures highly diluted in argon. Additionally, a set of data on the ignition delay times of diluted acetylene-air mixtures is presented.

DEDICATION

I would like to dedicate this thesis to my Dad, Juan Jose Vivanco Arriaga, my Mom, Belinda Gracia Nava and my sister, Belinda Amelia Vivanco Gracia for their unconditional love and support. They have been and will always be here when I need them most.

ACKNOWLEDGMENTS

I would like to thank my advisor and committee chair, Dr. Eric Petersen for sharing his time and knowledge with me. I know I would not have the opportunities I have today if it wasn't for the chance he gave me to work with him. I would also like to thank my committee members, Dr. Simon North and Dr. David Staack, for their time and support on this thesis. I would also like to acknowledge The Aerospace Corporation for donating the bulk of this facility to Texas A&M.

I also want to say thank you to all of my colleagues at the Petersen Research Group. I think we have a great group of people there and it was always fun to go to the lab. Special thanks go to Anibal Morones, Daniel Pastrich, James Anderson, Katie Latourneau and the facility manager at the Turbomachinery Lab, Mr. Ray Mathews, for the all the lifting and thinking we had to do to complete this project.

NOMENCLATURE

MW	Molecular weight
γ	Specific heat ratio
P	Pressure
T	Temperature
t	Time
τ_{ign}	Ignition delay time
$\frac{dp}{dt}$	Change in pressure over time
Φ	Equivalence ratio
Δt	Time interval measured by counters

Subscripts

1	Conditions at t = 0 in the driven section
2	Conditions after the passage of the incident shock wave
3	Zone behind the contact surface
4	Condition in the driver tube at t = 0
5	Conditions behind the reflected shock wave

Abbreviations

HPST	High Pressure Shock Tube
LPST	Low Pressure Shock Tube
NUIG	National University of Ireland at Galway

TABLE OF CONTENTS

Page

LIST OF FIGURES

Page

LIST OF TABLES

Page

CHAPTER I

INTRODUCTION

The International Energy Outlook 2013 projects that world energy consumption will increase by 56% between 2010 and 2040, and even though renewable and nuclear energy usage is rapidly increasing, fossil fuels are still projected to supply around 80% of the world's energy during that period. Along with this increase in fossil fuel usage comes an increase in emissions, of which 46% are due to carbon dioxide [1]. To meet the upcoming energy demands while also complying with stricter emissions regulations, combustion of all types of fuels needs to become cleaner and more efficient. To achieve both of these goals, there have to be improvements in several fields, including manufacturing and design, but more importantly in the area of chemistry. Understanding how the combustion event takes place, which species are most important in a particular scenario and at what conditions a fuel exhibits certain behavior all play an important role on combustion efficiency and pollutant emissions. Therefore, it is necessary to have an apparatus capable of measuring the combustion properties of a wide variety of fuels under relevant thermodynamic conditions.

Shock tubes have proved to be one the best tools to perform such measurements and have been used to improve the design and modeling of combustion processes. Shock tubes are ideal for such experiments because of their simplicity and reliability, and they have been used heavily for over 50 years to study physical and chemical processes at high temperature [2]. In a shock tube, it is possible to vary the temperature and pressure

of the experimental mixture over a wide range of conditions using a shock wave. A key feature of shock tubes is that for a short period of time (typically on the order of a few milliseconds), the pressure and temperature behind the reflected shock wave remain constant. During those few milliseconds and with the use of optical and/or diagnostics, it is possible to follow the progress of the combustion process [3]. Some of the most common applications of shock tubes in chemistry have been performing measurements of ignition delay times in gas-phase mixtures, elementary reaction rate coefficients, and spectroscopic data, among many others.

The purpose of this study was to assemble and validate a new shock tube facility that was donated to Texas A&M University from The Aerospace Corporation (Aerospace) in El Segundo, California. The donated facility was intended to be used in the area of chemical kinetics at its original location, and so in this work it is shown why it complies with the major design features required to perform accurate kinetics measurements. Some of the desired characteristics include a long, very smooth driven section with a large inner diameter and a long driver tube. This thesis provides an overall description of the facility including the major hardware pieces, software, and electronics used to perform experiments. In addition to the donated hardware, several systems had to be designed, manufactured and installed, these include a new high-vacuum system, gas delivery system, computer-based DAQ system and a shock velocity-measurement system that is critical in the calculation of experimental temperature. Once the facility was assembled and ready for testing, the pressure and velocity behavior of the shock tube were characterized and the details and results from this are shown in this thesis.

Additionally, a validation study was performed that involves replicating the demonstrated behavior of hydrogen and methane-based mixtures at various conditions. Also, the first set of new data for the ignition times of real acetylene-air mixtures was obtained using the new facility, and the results are presented herein.

CHAPTER II

BACKGROUND

Shock-Tube Physics

The first shock-tube experiments were performed as early as 1899 by French scientist Paul Vieille, in which he mainly experimented with different diaphragm materials and driver gases. But it wasn't until 1946 when Payman and Shepherd published the first major article on the shock tube [4]. In this work, they cover the essential features of the modern shock tube and some of its possible applications. They also identified some of the major parameters that influence a shock tube experiment such as diaphragm thickness; length of the driver and driven tubes; and molecular weight of the driver gas. For more details on the history of shock-tube development, refer to the well-known text on shock tubes by Gaydon and Hurle (1963).

Since around 1953 there has been a steady stream of studies reporting new applications for shock tubes in fields such as aeronautics, physics, and chemistry [3]. Some of the reasons why shock tubes are widely used tools in these areas are because in a shock tube, the test mixture is brought to experimental conditions almost instantaneously; the conditions are highly repeatable and it is possible to get any combination of temperature and pressure within the limits of the particular facility. The experimental conditions behind the reflected shock wave (without any driver-gas

tailoring) can be maintained for a few milliseconds, during which several different kinds of measurements can be performed.

A simple shock tube is comprised of two main tube sections, the driver (high pressure) and the driven (low pressure), which are separated by a diaphragm. The driven tube is filled with the gas mixture that will be studied and it typically contains a fuel, an oxidizer, and a diluting gas. The driver tube is traditionally filled with a single species but it can also be a combination of gases depending on the type of experiment that is necessary. The gas in the driver tends to be an inert gas with a high speed of sound since the higher the speed of sound in the driver gas the stronger the shock wave [3]. The driver tube is pressurized until it reaches a pressure high enough to rupture the diaphragm and, typically, the pressure difference across the diaphragm is between tens to hundreds of times higher on the driver side. When the diaphragm finally ruptures, the high pressure differential and resulting motion of the driver gas into the driven section creates a shock wave, called the incident shock wave, which propagates through the driven gas. As the incident shock passes through the low-pressure mixture, the temperature and pressure of the mixture are increased nearly instantaneously (on the order of a microsecond or less). The timescale of this heating process is one of the main attributes of shock tubes. Since the mixture is brought to the high-temperature conditions within a few microseconds, issues such as heat transfer are avoided.

Figure 1 shows a schematic of the new facility at Texas A&M University along with an x-t diagram used to describe visually the different waves generated inside the shock tube. Using the conventional nomenclature, the initial conditions are depicted by

zone 4 (T_4, P_4) for the driver tube and zone 1 (T_1, P_1) for the driven tube. Zone 4 is typically filled with an inert, single-species gas or mixture of gases with a low molecular weight MW since driver gases with a high sound speed are desired. For this reason, the most commonly used gases to drive a shock wave are hydrogen and helium. Zone 1 is filled with the gas mixture that will be exposed to the high-temperature, high-pressure region to be studied.

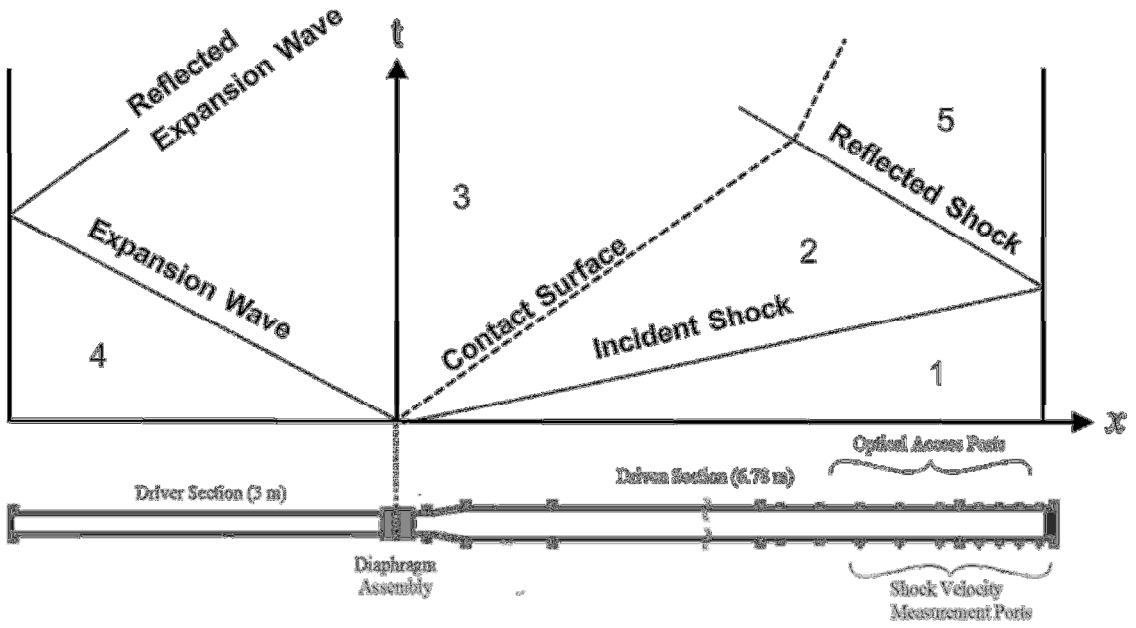

Figure 1. Classic x-t diagram of a shock tube accompanied by a schematic of the new shock-tube facility described in this work.

When the diaphragm breaks, the incident shock wave travels along the driven side increasing the temperature and pressure to T_2 and P_2. The extent of the increment in temperature and pressure depends on how strong the shock wave is, which can be characterized by the Mach number of the shock wave. For a typical experiment in the

facility described in this work, the average Mach number is about 3. Shock waves with this Mach number yield an increase in temperature of about two or three times T_1.

After some time, the incident shock wave reaches the end of the driven section (endwall) and it reflects back into the previously heated gas mixture. The strength of the reflected shock wave is less than the incident shock but the temperature and pressure are increased once more, to T_5 and P_5. This second increase in thermodynamic conditions is, again, about twice that of T_2 and P_2. In this high-temperature and high-pressure region, zone 5 in Figure 1, the mixture is quiescent and at (ideally) constant temperature and pressure. These constant thermodynamic conditions are held for a few milliseconds and it is during this time that combustion processes take place under ideal conditions for observation.

The observation period is the time between the reflection of the shock wave and the interaction of the reflected shock with any other wave that could disturb the conditions in zone 5. There are two other waves that the reflected shock could interact with and these are: the contact surface and the rarefaction fan. The contact surface travels behind the gas following the incident shock wave, and it is shown in Figure 1. The contact surface separates the high-pressure gas and low-pressure gas and it is usually assumed that there is no gas flow across this interface. The rarefaction fan is a set of expansion waves that are generated at the time of the rupture of the diaphragm and propagates back into the driver gas. The leading expansion wave moves at the speed of sound of zone 4, and subsequent waves travel slower since the driver gas has been cooled by the leading expansion wave. The expansion waves reflect off the endwall of

the driver side and travel into the driven side; and depending on the driver gas and shock tube geometry it may or may not catch up to the contact surface before the contact surface interacts with the reflected shock. The interaction of either of these two waves with the reflected shock wave disrupts the conditions in zone 5 and marks the end of the observation time.

There are several techniques that can be used to delay the arrival of both the contact surface and the expansion waves to increase the observation time. For example, in some cases it is possible to shorten the driven tube and extend the driver tube. This tube-length modification would delay the arrival of the expansion wave to the region behind the reflected shock wave. When modifying the facility is not possible, the most common approach to extend the observation time is to utilize a driver-gas tailoring method. Since the leading expansion wave travels at the speed of sound in region 4, a gas or mixture of gases with a low specific heat ratio γ and/or high molecular weight MW would result in a lower speed of sound and thus the rarefaction fan would slow down.

Shock Tubes at The Petersen Research Group

Prior to this thesis, the Petersen Research Group has had access to three shock-tube facilities: two at Texas A&M University (TAMU), the Lower Pressure Shock Tube (LPST) and the High Pressure Shock Tube (HPST); and one at The Aerospace Corporation. The LPST has a 4 in by 4 in driven section, it is heatable to 200 °C, and it

is possible to achieve reflected-shock-pressures of up to 10 atm. It is used primarily for aerosol experiments and, with a recent addition of a unique driven section with large viewing windows, it is now also used to perform dust-layer experiments where the height of a dust column is measured after the passage of a shock wave. The HPST has a driven section of 4.7 meters long with a relatively large inner diameter of 15.24 cm with the capability of obtaining reflected-shock conditions of 800-4000 K and up to 100 atm. It is used primarily for fuel-air ignition and dilute kinetics measurements. The (remaining) shock tube at The Aerospace Corporation has a driven section of 10.2 meters long, it is heatable to 200°C, and it is able to achieve conditions in a similar range to the HPST. This facility is used for laser diagnostics, kinetics, and ignition measurements. Even with access to two shock-tube facilities at A&M and the use of the facility at Aerospace, there is still the need for an additional facility with similar capabilities as the HPST. This addition would allow the performing of different types of experiments simultaneously without having to change the set-up as it is the case with only one high-pressure shock tube.

New Chemical Kinetics Shock Tube

A shock tube to be used for chemical kinetics needs to have certain attributes to ensure the measurements are as accurate as possible. Although there are several factors that contribute to the accuracy of kinetics measurements, the experimental temperature is one of the most important. For example, a small error in the temperature (~1%) could

lead to a large error (~25%) in the Arrhenius rate of a particular reaction [5]. Typically the experimental temperature (and pressure) is not measured directly but rather calculated using the well-known gas dynamics relations for normal shock waves that depend on the velocity of the incident shock wave and the initial conditions, T_1, P_1 and test-mixture composition. For this reason, measuring the velocity of the incident shock wave becomes the key step towards obtaining accurate experimental conditions.

Measuring the velocity of the incident shock wave would be a simple matter if the velocity could be assumed to be constant. Unfortunately, this ideal scenario is not the case, and there are several non-ideal phenomena present at the shock front and within the column of gas that follows the incident shock. In addition to the physical phenomena, errors could also arise due to the instrumentation used, but this type of error is addressed in a later chapter. The most-relevant, non-ideal effect in a typical experiment is the formation of a sidewall boundary layer immediately behind the incident shock wave. The boundary layer represents a problem for two reasons: first, the formation of a boundary layer affects the uniformity of the gas into which the shock will be reflected. As a result, the reflected shock propagates back into a flow field that is moving slower within the boundary layer than in the center of the tube. This disparity can contribute to bifurcation of the reflected shock near the wall. The second reason why the boundary layer is a problem is that it contributes to incident-shock attenuation. This axial decrease in incident shock velocity causes the temperature behind the incident shock to be non-uniform, and this non-uniformity will be even greater when the reflected shock passes back through the test mixture. Additionally, since the velocity of the incident shock

immediately before reflection is the key parameter to determine the experimental conditions, the shock attenuation needs to be taken into account when measuring the velocity. For example, if the velocity of the shock were measured at only one location, the measured velocity might not represent the true value immediately before reflection.

A shock tube that will be dedicated for chemical kinetics experiments needs to be designed with these types of non-ideal phenomena in mind to minimize the uncertainty of the experimental-condition calculations. The facility donated by Aerospace was originally part of a facility with two identical shock tubes (the main tube is mentioned above). An overview of the original facility and some of the measurements performed with it can be found in Petersen (2005) [5]. Being originally designed to perform several types of experiments, including kinetics measurements, the new facility possesses key features that are well suited for the type of measurements that will be performed at TAMU. First, the lengths of the driver and driven tubes provide an observation time of around 2.5 milliseconds using helium as the driver gas. This period for observation is enough for most kinetics experiments; however, it is possible to extend the observation time through the use of unconventional driver-gas mixtures. Amadio et. al. [6] is an example of using mixtures of C_3H_8/He and CO_2/He as driver gases to obtain test times of up to 15 milliseconds.

Also, since minimizing the boundary layer growth behind the incident shock plays a crucial role on the accuracy of the experimental conditions, several design features were implemented when designing the driven section. According to Bowman and Hanson 1979 [7], it is recommended that a relatively large diameter (> 5 cm) driven

tube is used to minimize the proportion of the incident-shocked gas that is affected by the boundary layer. The current facility has a 16.2 cm inner diameter and in addition to this, the surface finish was machined to a roughness of 1 μm or better. Additionally, Gaydon and Hurle [3] recommend that measurements be made very close to the endwall in a shock tube that has a low length-to-diameter ratio (< 50). The new facility has a length-to-diameter ratio of 42, falling within the recommended range. All the measurements are performed at 1.6 cm from the endwall which is sufficiently far away to minimize heat transfer effects with the endwall but close enough to ensure that flow conditions are as close to ideal as possible.

CHAPTER III

SHOCK-TUBE FACILITY DESCRIPTION

The shock-tube facility consists of hardware, software, a high-vacuum system, a gas-handling system, and a shock velocity-measurement system. An overall view of the facility and the main connections between systems are shown schematically in Figure 2 . The donation from Aerospace included the main hardware pieces: driver tubes, driven tubes, sidewall ports, endwall cap with no ports, vacuum chamber and supports to secure the facility in place. The rest of the necessary items were either purchased or fabricated in house. Among these items were: the diaphragm package and cutter, endwall ports, and vacuum components. In addition to the hardware, all the electronics and gas handling systems had to be designed, purchased, assembled, and tested. An overview of each of the systems is given herein.

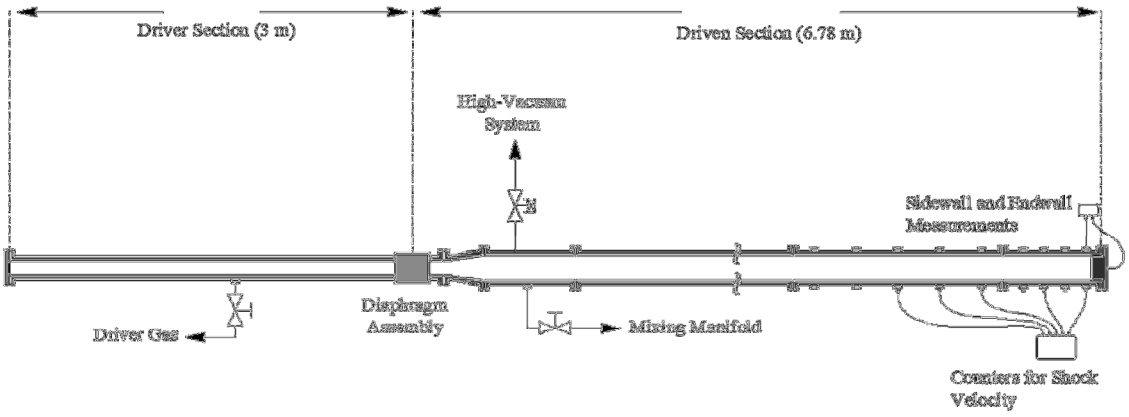

Figure 2. Schematic of new shock-tube facility showing main tube sections and additional systems installed on the facility.

The driver tube consists of two 1.52-m tubes made of SAE 4340 forged steel, with an ID of 7.62 cm and a 1.27-cm wall thickness. The driven tube, in the current set-up, consists of three tube sections and an endwall cap. All the driven-tube sections are made of 304 stainless steel, with an ID of 16.2 cm and a 1.27-cm wall thickness. All inner surfaces of the driven tube are polished to a surface finish of 1-μm RMS or better to minimize boundary layer growth. The first driven section is 4.57 m long, the second section is 1.52 m long, and the third section is 68.58 cm long. The layout shown in Figure 2 has a total length of 10.78 m, but it is possible to add or remove a section to adjust the length depending on the experiment needed. The driven sections are connected via weld-less flanges designed specifically for high pressure and to minimize perturbations to the flow. The design of these connections is described in more detail by Petersen (2005) [5].

One of the necessary features of a shock tube is the ability to have optical access to what is happening inside the tube without perturbing the flow or combustion process. To do this, the last two sections of the driven tube have 28 access ports located on the sidewall at set distances. These ports allow the performing of non-intrusive measurements along the sidewall, commonly with some form of optical diagnostic, so the combustion characteristics of a given mixture can be studied. Although the ports are simple plugs, extreme care has to be taken during the manufacturing process. The sidewall ports for example have to follow the curvature of the inner diameter of the shock tube to prevent the ports from causing disturbances on the flow when the shock wave passes by. Also, when installing any sort of instrumentation in the ports, it is

necessary to install it in such a way that it is flush with the shock tube's inner surface. An example of the sidewall ports being used for pressure transducer is shown in Figure 3.

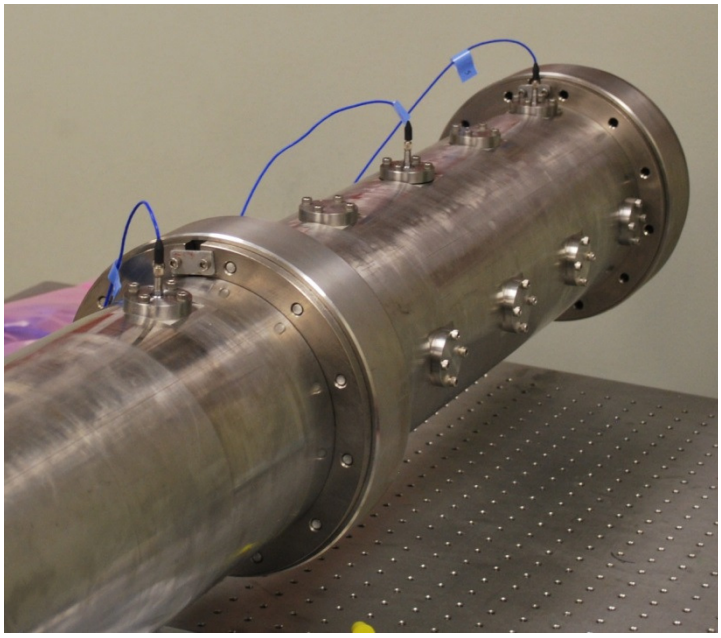

Figure 3. Sidewall ports on the last two sections of the driven tube with pressure transducers installed.

Several additions had to be done to the endwall assembly, including the fabrication of the endwall ports. A schematic of the endwall assembly is shown in Figure 4. The endwall assembly is comprised of the outer section, the cap, and the access ports. The outer section is bolted to the cap to make the endwall insert seen in Figure 4 and the insert extends inside of the driven tube. The distance from the endwall to the closest sidewall port was modified from what it was when the facility arrived. This effective repositioning of the endwall was accomplished with an aluminum spacer fabricated in

house to place the endwall at 1.6 cm from the closest sidewall port. This distance is what has been used in the past on the other Texas A&M shock tubes.

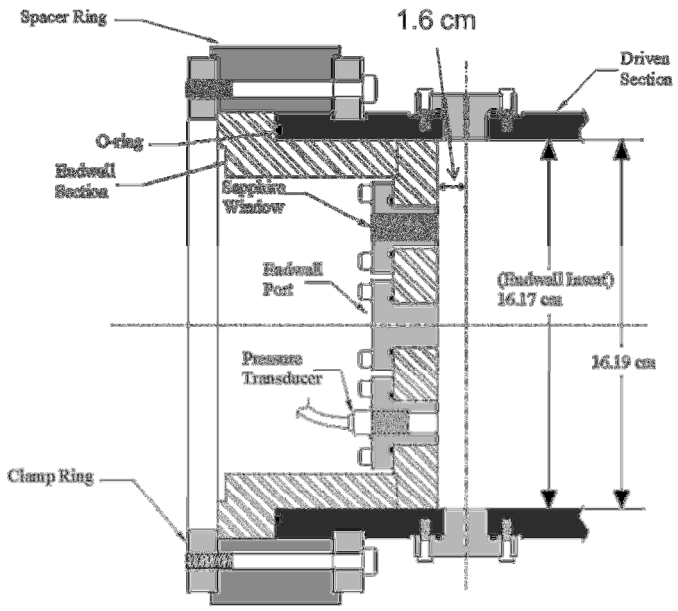

Figure 4. Schematic of endwall assembly highlighting its main components.

After the rupture of the diaphragm, the incident shock wave propagates through the driven tube gas with a given velocity. The magnitude of the shock's velocity along with the initial pressure and temperature are what determines the experimental conditions behind the reflected shock wave for a particular experiment. Thus, it is of extreme importance to measure the velocity of the incident shock wave as accurately as possible. The velocity of the incident shock is measured using 5, fast-response, piezoelectric pressure transducers (PCB 113B22) installed along the sidewall of the driven tube. These transducers trigger four Fluke/Phillips PM6666 high-frequency interval timers that measure the time it takes for the shock wave to pass by a pair of

transducers. With this time interval and the distance between transducers, the velocity of the incident shock wave is measured at 4 intervals, and it is curve-fitted to extrapolate the velocity to the endwall when the incident shock reflects back. The accuracy of this measurement has a big impact on the experimental conditions and comments on the uncertainty of this measurement are addressed in following chapter.

To test under high-purity conditions, a high-vacuum system with an ultimate pressure lower than 10^{-6} torr was installed for the facility. The vacuum chamber is connected to the driven section in two ways: the first is through a half-inch manual valve that is used to avoid overloading the roughing pump at the beginning of the evacuation process, and the second is through a 25.4-cm ConFlat flange that has a pneumatic poppet-valve of 12.7 cm in diameter. The poppet valve is opened when the pressure in the driven section is low enough that the roughing pump can pull through a bigger opening. The poppet valve plug was precision-machined to match the circumference of the driven tube and avoid causing any obstructions to the incident shock wave. To start, the driven section is vacuumed down to around 80 mtorr using an Agilent DS602 (605 L/min) roughing pump. Once the system is at 80 mtorr, an Agilent Turbo-V1001 turbo molecular pump, backed by an Agilent DS402 (410 L/min) backing pump, is opened to the system via a 25.4-cm gate valve and brings the system down to a pressure of 10^{-6} torr or lower. The pressure in the system is monitored using two MKS Baratron capacitance manometers model 626B (0-10 torr and 0-1000 torr) and with an Agilent MBA-100 ion gauge for high-vacuum applications. At the same time, the driver tube is evacuated using an Agilent DS102 (114 L/min). Leak rates are performed routinely to verify that the leak

rate is still within an acceptable range. For high-vacuum conditions (< 1mtorr), a leak rate of 0.216 mtorr/min was measured for the driven section. However, the driven tube is typically at a much higher pressure than that (1 -100 torr) so the driving force for a leak is much lower than under high-vacuum conditions. A typical leak rate 0.218 mtorr/min was found when the driven pressure was at 10 torr. Since running an experiment after filling takes under a minute, the impurities coming into the tube can be neglected with the above leak rate. Using this vacuum system, a turnaround time (time from breakage of a diaphragm to the next) of between 25-30 minutes is possible for low-pressure experiments.

Another important addition to the facility was the diaphragm package, which is the assembly that holds the diaphragms in place to separate the driver and driven sections. A schematic of the diaphragm package and breech loader mechanism used to mount the diaphragm assembly is shown in Figure 5.

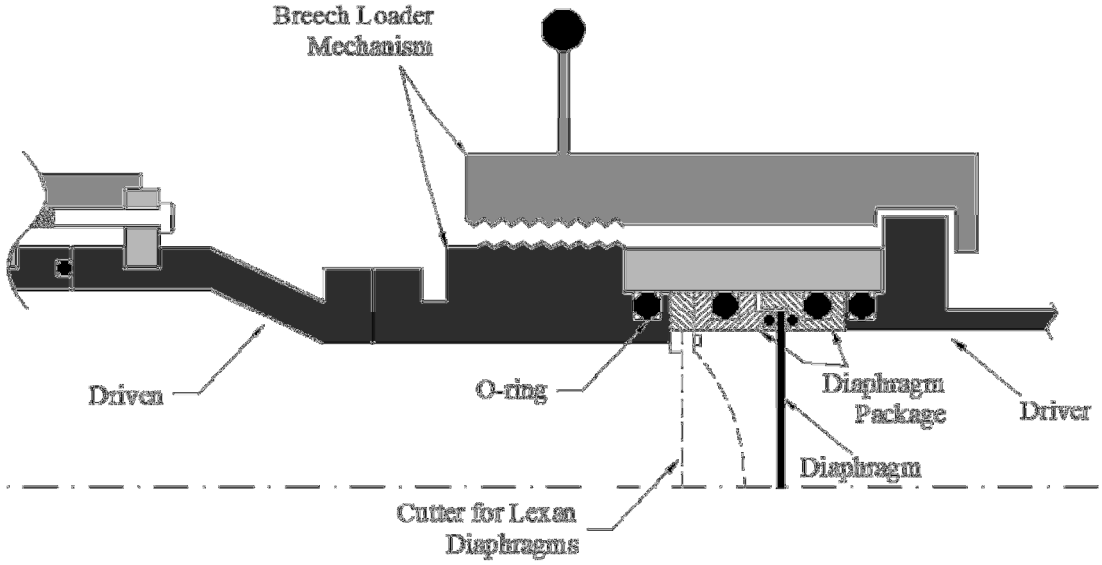

Figure 5. Schematic of the mechanism to attach the diaphragm package to the driven and driver tubes.

The facility utilizes both lexan and pre-scored aluminum diaphragms, depending on the desired testing pressure. For test pressures below 10 atm, lexan diaphragms are used along with a cutter blade designed to facilitate rupture and to increase breakage repeatability. The aluminum diaphragms are used for pressures greater than 10 atm and up to 100 atm. The diaphragm package is comprised of a sleeve, two inserts, and the optional cutter. All the pieces are made of stainless steel, and all were fabricated in house except for the sleeve. The diaphragm is placed between the two inserts. Each insert has two o-rings, one facing the diaphragm and one on its circumference. The CAD model for one of the two insert pieces is shown in Figure 6.

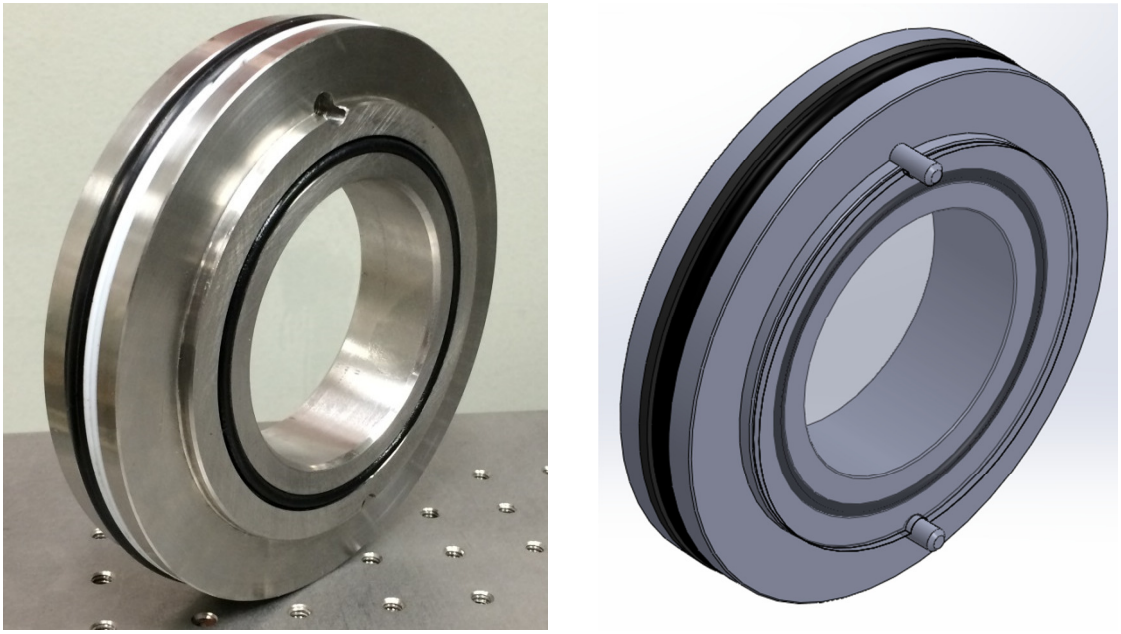

Figure 6. Comparison between the CAD model and in-house fabricated part of one of the two diaphragm-package inserts.

The face o-ring presses against the diaphragm to make a seal. The inserts slide into the sleeve, and the o-rings on the circumference create a seal that separates the tube from ambient air; this can be seen in Figure 5. The sleeve is then mounted on the driven section and sealed with the breech loader mechanism.

CHAPTER IV

SHOCK-TUBE CHARACTERIZATION

The behavior of each shock-tube facility is slightly different and depends on many things including geometry, electronic equipment used, and overall design intent. Thus, it is important to characterize the behavior of the new facility in several areas and to make sure it is the expected behavior before utilizing it to perform experiments. By behavior of the shock tube, it is meant the sidewall and endwall pressure, vacuum integrity, turnaround times between experiments, and axial velocity profile of the incident shock wave. Each of these areas are discussed and validated in the following subsections.

Pressure Behavior

Pressure is a key parameter for a shock-tube experiment, and it needs to be monitored for every experiment. As it was noted previously, one of the attributes of performing measurements behind the reflected shock is the fact that the thermodynamic conditions stay constant. It is necessary to verify the quiescent, constant-property conditions by observing the pressure behavior at the locations where future measurements will be made. The endwall pressure measurements are performed with a fast response, piezo-electric transducer (PCB 113B22) with a time response of $< 1\mu$sec. It is connected to an amplifier box (PCB 482C15) for signal conditioning via a 3 meter,

low-noise coaxial cable (PCB 003C10). Figure 7 shows a typical endwall pressure trace obtained from a mixture of stoichiometric CH_4 in air (air refers to 21% O_2 and 79% N_2 throughout this work) at a reflected–shock pressure of 2.1 atm and temperature of 980 K. As it can be seen from Figure 7, the endwall pressure transducer is able to record a very clean signal with a high signal-to-noise ratio. Also the increase in pressure from the reflected shock wave happens within a few microseconds (basically the passage time of the shock wave over the sensor), and this rise time is validated by the recorded pressure trace. To verify that the pressure stays constant for the duration of the experiment, the rise in pressure over time, dp/dt, was calculated.

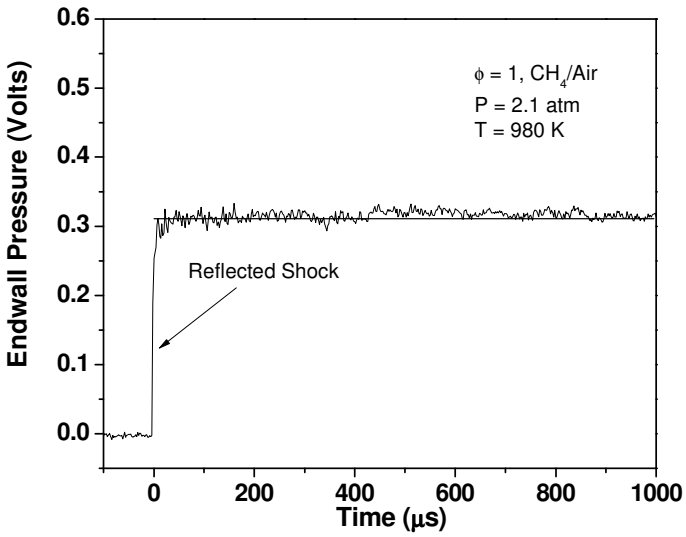

Figure 7. Endwall pressure trace showing the negligible increase in pressure during the test time for a stoichiometric CH_4/Air mixture at given conditons.

For this particular case, it came out to be around 0.4%/ms, which equates to an increase of 0.0084 atm/ms. As a rule of thumb from the other facilities at TAMU, a dp/dt

of 2%/ms or less is commonly acceptable, therefore the value obtained from Figure 7 is more than acceptable. In addition, the general 2%/ms attenuation corresponds to an increase in temperature of about 0.45%/ms. For the example provided above, the 0.4%/ms attenuation from Figure 7 corresponds to a 0.9 K/ms which is an almost negligible rate of temperature increase since the test time of the facility is about 2.5 – 3 milliseconds.

The sidewall pressure measurements are performed with a high frequency sensor (Kistler 601B1) with similar specifications as the endwall transducer. It has its own signal conditioner box (Kistler 5010B1) and they are connected via a 2-meter, low-noise coaxial cable (Kistler 1631C2). Figure 8 shows the sidewall pressure trace from an observation port located 1.6 cm away from the endwall for an experiment with a mixture of stoichiometric H_2/O_2 highly diluted in Argon at 0.87 atm and 2589 K. In this case, the arrival of the incident shock wave is observed followed by the passage of the reflected shock going in the opposite direction.

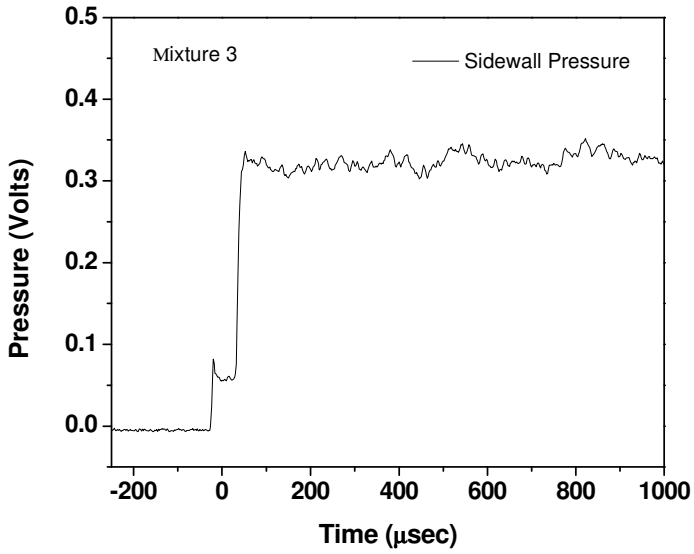

Figure 8. Representative sidewall presure trace showing low increase in pressure during the test time for H_2 highly diluted in Ar at 0.87 atm and 2589 K.

From looking at both the endwall and sidewall pressure signals over the wide range of temperatures in Figs 7 and 8, it can be concluded that the pressure remains relatively constant for a sufficient amount of time to perform typical high-temperature chemical kinetics measurements.

Next, it is important to determine what the observation time is for the current configuration of the facility, detailed in Chapter III. For the length of driver and driven tubes currently in use with helium as a driver gas, the observation time is close to 3 milliseconds. Figure 9 shows the sidewall pressure trace recorded for Argon at 1.8 atm and 1555 K. From Figure 9, it can be seen that after about 3 milliseconds, the pressure starts decreasing due to the arrival of the leading expansion wave at the observation port where the sidewall pressure sensor is located.

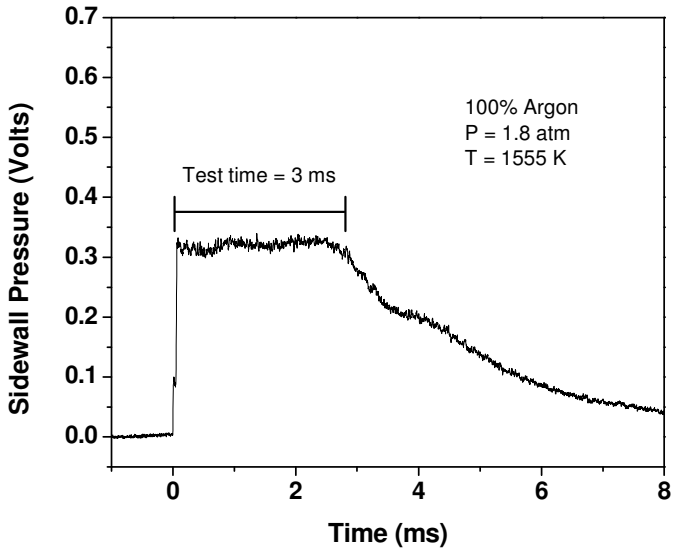

Figure 9. Sidewall pressure trace illustrating the observation time behind the reflected shock wave for the current set-up of the new shock-tube facility.

Incident Shock Velocity Measurement

It was already mentioned that the velocity of the incident shock wave is used to determine the experimental conditions. But, it is not sufficient to only know the velocity of the shock wave at the instant of reflection; it is also necessary to observe how the velocity is changing along the driven tube. Most of the time, the incident shock wave attenuates as it propagates along the tube due to viscous effects or imperfect rupture of the diaphragm. The degree of attenuation will determine how large the discrepancies in experimental conditions are behind the reflected shock wave.

In the new facility, the average speed of the shock wave is measured for several distance intervals over roughly the last 1.8 meters of the driven section. To make this measurement possible, the technique used takes advantage of the fact that the shock wave induces significant changes in pressure. Thus, by monitoring the changes in pressure, it is possible to identify the instant at which the shock wave passes by a given location. Figure 10 shows a schematic of an example of the set up used to perform the speed measurement. In this example there are four piezo-electric pressure transducers with a response time of < 1μsec positioned at specific distances. As the incident shock wave passes by each of them, the transducers detect the rise in pressure and send a voltage signal to three counter boxes. The counters act essentially as a very accurate stop-watch that is started and stopped by the signal received by a pair of pressure sensors.

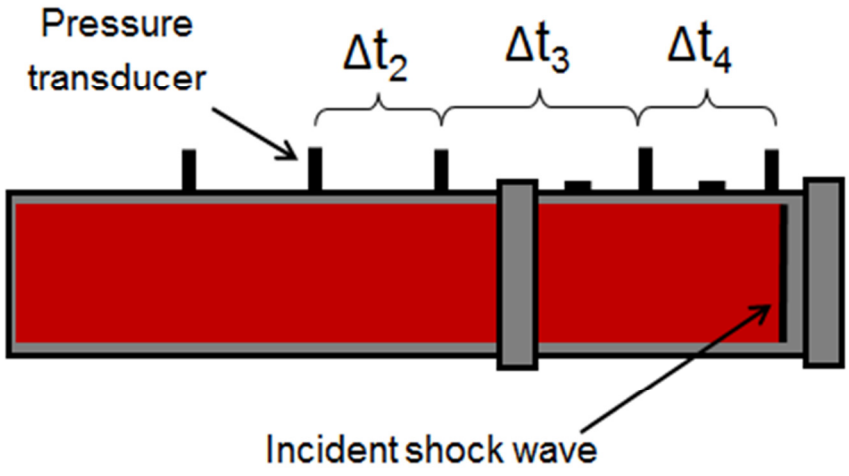

Figure 10. The pressure transducers detect the abrupt rise in pressue behind the incident shock wave and trigger the timers.

Once the shock has passed by a pair of sensors, the corresponding counter box outputs the time it took the shock wave to travel the given distance. To first verify that the counters were giving accurate times, the pressure sensors were connected to a high-speed DAQ system with a resolution of 14 bits and a sampling rate of 10 MS/sec for each channel. The pressure trace from each transducer was recorded and plotted to measure the time interval manually. Then, the experiment was repeated and the time intervals were obtained via the counter method. The times for both methods were compared and the difference was less than 0.5%. Figure 11 shows the signal from each of the transducers in Figure 10. This step was performed to verify that the timers were measuring accurate times.

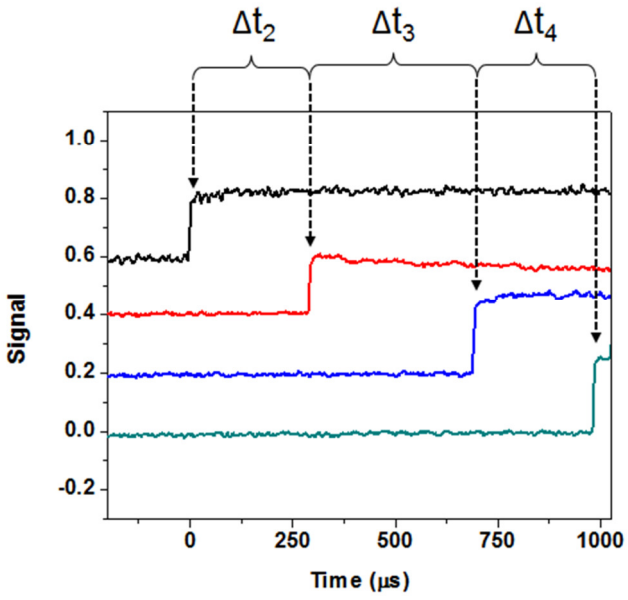

Figure 11. The counters get triggered at a user-specified voltage threshold and measure the time between succesive pressure transducers.

Figure 11 shows the signal from each of the transducers in Figure 10. This step was performed to verify that the timers were measuring accurate times. Once the time intervals are obtained, it is possible to calculate the velocity of the shock at three locations. The velocity points are then curve-fitted to observe the profile of the velocity and it usually follows a linear profile with a negative slope. Figure 12 shows an example of the velocity profile obtained for Argon as the test-gas for experimental conditions of 1753 K and 2.29 atm. The velocity-measurement set-up covers close to 1.8 meters of the driven section and it shows an attenuation of 1%/m. It is the longest possible distance that could be used for measuring the speed of the shock wave based on where the sidewall ports are located. This profile shows that the shock's velocity does in fact decrease linearly over roughly the last 2 meters of the driven tube.

The next step was to implement the best velocity-measurement set-up that yields highly repeatable and accurate measurements. While still being at The Aerospace

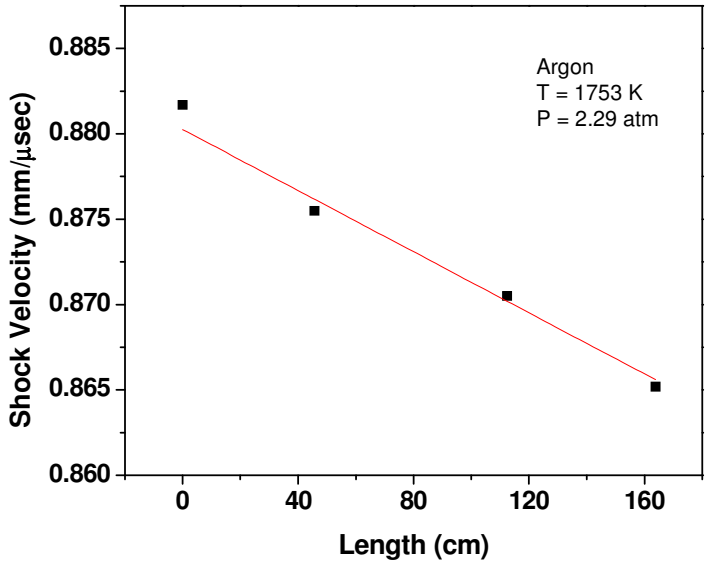

Figure 12. Example of the incident-shock velocity profile for the last 1.8 meters of the driven section.

Corporation, the two shock tubes (Chapter II) were utilized to perform an extensive uncertainty study of the velocity-measurement technique [5]. It involved measuring the speed of the shock wave for a wide range of experimental conditions while using several different distance intervals for the pressure transducers. The idea behind the uncertainty analysis was to identify the set-up that could provide velocity measurements that were as accurate and repeatable as possible, which translates to a very accurate calculation of the reflected-shock conditions.

To obtain the speed of the shock wave between any two points, it is necessary to know only two things: time and distance. The uncertainty study focused on finding the possible sources for error in the measurement of the distance between pressure transducers and the time measured by the counters. The main sources for error accounted

for in the study are discussed next, and the results of the uncertainty study are applied to the new facility to determine the best set-up.

The sources of error for the distance measurement include the size and location of the sidewall port; the size and location of the holes for the transducers; and the size and location of the mounting holes. The geometry of the driven section, the holes for the sidewall ports, and the location of the holes on the new facility are identical to the ones on the shock tube used for the previous uncertainty study, thus the source of error for the distance measurement is the same as for both shock tubes. Additionally, the electronic equipment (counters, amplifiers, cables, and pressure transducers) used for time measurement have the same specifications. Since both the time and distance are obtained the same way in the new facility as in the previous uncertainty study, the results are directly applicable to the new facility at TAMU. It was found by Petersen et al. (2005) that the inaccuracy of T_5 calculated from the velocity measurement increases as the test temperature increases and as the transducer spacing of the set-up decreases. Figure 13 shows a schematic of the last two sections of the driven tube with the available locations for sidewall ports.

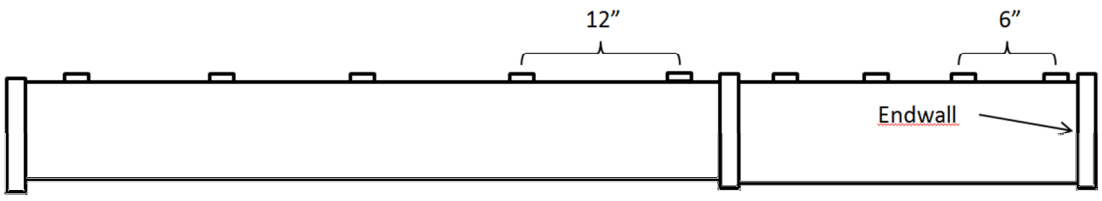

Figure 13. Schematic of the last two driven tubes showing 4 places of 12” and 3 places of 6” available to install pressure transducers.

As it can be seen, there are a lot of possible transducer spacings, but there needs to be a compromise between measuring a large enough portion of the tube to obtain a better estimate of the true shock attenuation and having transducers close to the endwall since the velocity at the endwall is most important in terms of calculating reflected-shock conditions. The 6-in spacing closest to the endwall has an uncertainty of about 15 K, which is too high for the type of measurements to be performed with this facility. The next possible spacing (12 in) yields an uncertainty of < 10 K for up to 2200 K, and since most experiments will be below this temperature, 12 in is the best option closest to the endwall. The rest of the transducers were positioned in a way that the velocity could be measured for at least 1 meter before the endwall. The reason for this is that attenuation rates are typically presented in % attenuation/meter, and it seemed appropriate to try to cover at least that distance. Figure 14 shows the final transducer set-up for the velocity measurement. This setup was selected after trying three other arrangements, but the chosen set-up showed the highest repeatability among all the spacings tried.

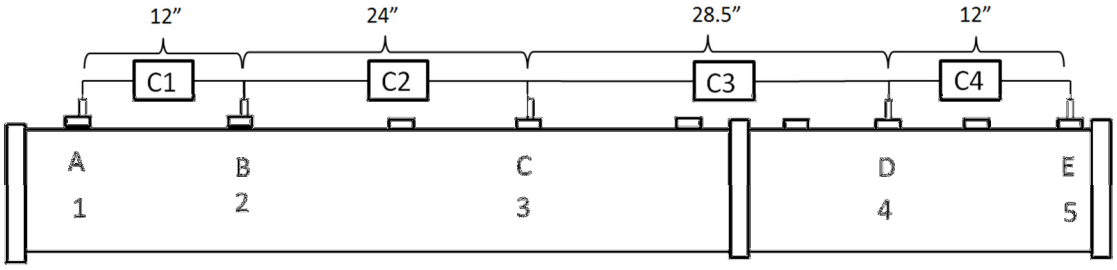

Figure 14. Schematic of the final set-up to be used for the shock-velocity measurement.

This set-up provides two 12-in intervals, one 24-in interval, and one 28.5-in interval. On average, the observed attenuation rate was around 1 – 1.5 %attenuation/meter. Figure 15 shows a velocity profile using Argon as the test-gas at 1778 K and 4.74 atm with an attenuation rate of 1%/meter. Also shown is the uncertainty for each velocity point.

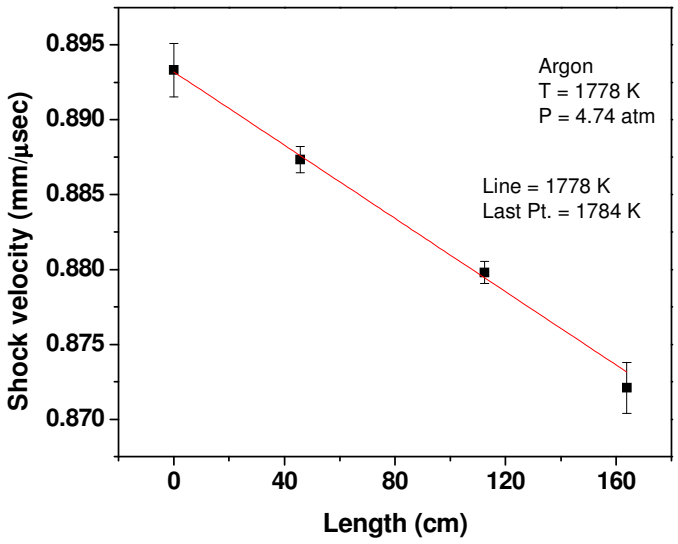

Figure 15. Typical velocity profile for the new shock tube facility. The attenuation of the shock is linear and falls within the uncertainty of each point.

The profile in Figure 15 represents the best-case scenario where the linear fit falls well within the uncertainty of each measured point. When this correspondence is the case, the temperatures obtained using the last velocity point or the linear fit through all the points differ from one another by 6 K, or 0.3%. However, sometimes the velocity points exhibit a highly non-linear behavior which may be attributed to a secondary non-ideal shock formation/propagation effect or vibration that perturbs the trigger signals [5].

An example of such non-linear behavior can be seen in Figure 16. Even though the velocity profile is not linear by visual inspection, a linear fit through the measured points still yields reasonable results. This idea is supported by the fact that even using the profile in Figure 16, the velocity using the linear fit or the last velocity point both yield temperatures that differ from one another by only 0.25% or about 4 K. On average, the difference in the temperature calculation using a velocity profile that is non-linear is about 0.2 – 0.5% of the temperature using the last velocity point. Only in rare instances were the velocity points uncertain enough that the experiment had to be repeated.

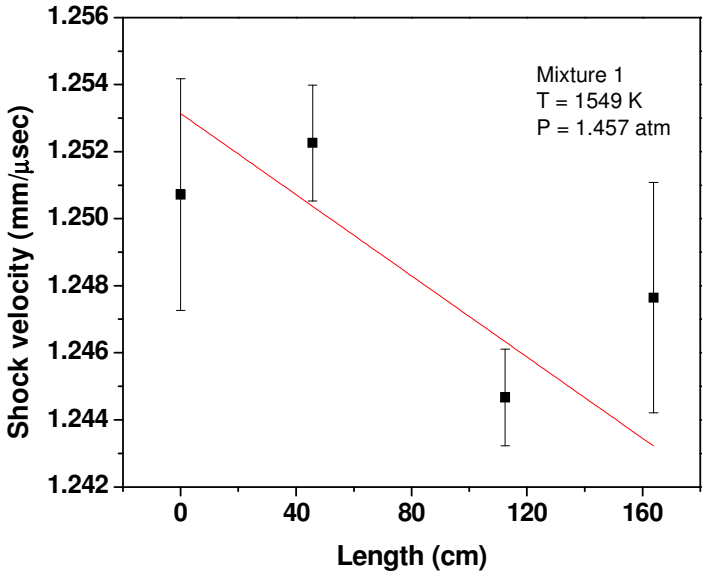

Figure 16. Example plot of a velocity profile that exhibits a non-linear behavior.

CHAPTER V

SHOCK-TUBE VALIDATION STUDY

In the previous chapter, it was proven that the new shock-tube facility has the capabilities to perform accurate and repeatable experiments. In this chapter, the details and results of a study performed to validate the data obtained with the new facility are presented. The validation study involved replicating the behavior of well-studied fuels and comparing the experimental data with current models. Table 1 shows the mixtures selected for the validation study. The study combines diluted and non-diluted hydrogen and methane-based mixtures at an equivalence ratio, ϕ, of 1. These mixtures were selected because they have been studied extensively, and the current models provide excellent predictions for the ignition times of these fuels over a wide range of conditions. All mixtures were prepared using the partial pressure method in a separate mixing tank that was evacuated to a pressure of $< 10^{-5}$ torr prior to the preparation of each mixture.

Table 1. Composition of mixtures of fuel - air/oxidizer used for the validation study.

Mix	Fuel	Dilution	ϕ
1	CH_4	71% N_2	1
2	CH_4	97.5% Ar	1
3	H_2	98% Ar	1

Ignition delay time (τ_{ign}) is one of the parameters that is typically used to compare experimental data with the chemical kinetics models. Ignition delay times of

each mixture were obtained at low pressures and a wide range of temperatures. It is important to first take a look at how the pressure and emission traces look for each of the mixtures and assess the quality of the signals. Figure 17 shows the endwall pressure trace obtained from mixture 1 in Table 1 at a reflected-shock pressure and temperature of 1.68 atm and 1498 K, respectively. The increase in pressure due to the reflection of the shock wave is clearly depicted, followed by the constant pressure period between reflected-shock conditions and the ignition event; and lastly, the ignition event is also captured in the trace showing a distinct rise in pressure that can be used to determine τ_{ign}. Details on why the endwall pressure is the important parameter to follow for this particular mixture are addressed in the following subsections.

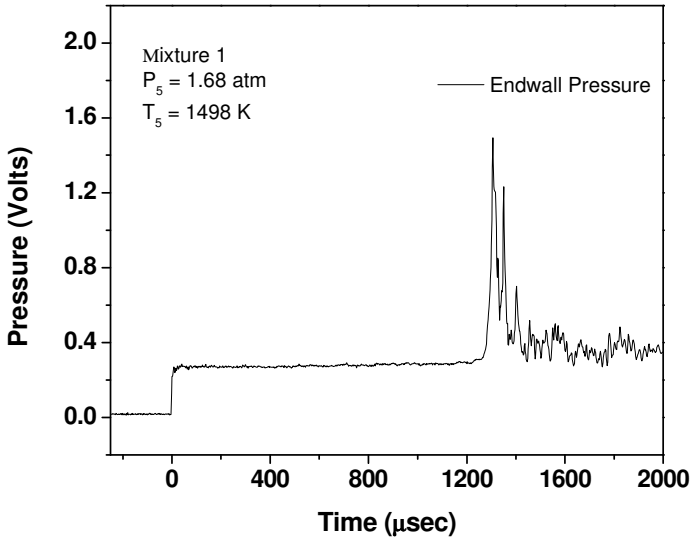

Figure 17. Representative endwall pressure trace for non-diluted ignition from mixture 1 of this work.

Figure 18 shows representative sidewall pressure and emission traces obtained from mixture 2 in Table 1 for reflected-shock conditions of 2.47 atm and 1821 K. The details on how the emission trace is obtained are explained in the next subsection of this chapter. The time of passage of the incident and reflected shocks are easily identified and the pressure behind the reflected shock stays relatively constant for the duration of the experiment. The emission profile looks as expected, where the time of formation and depletion of the species of interested (OH* in this case) is clearly shown. The emission trace also shows a high signal-to-noise ratio.

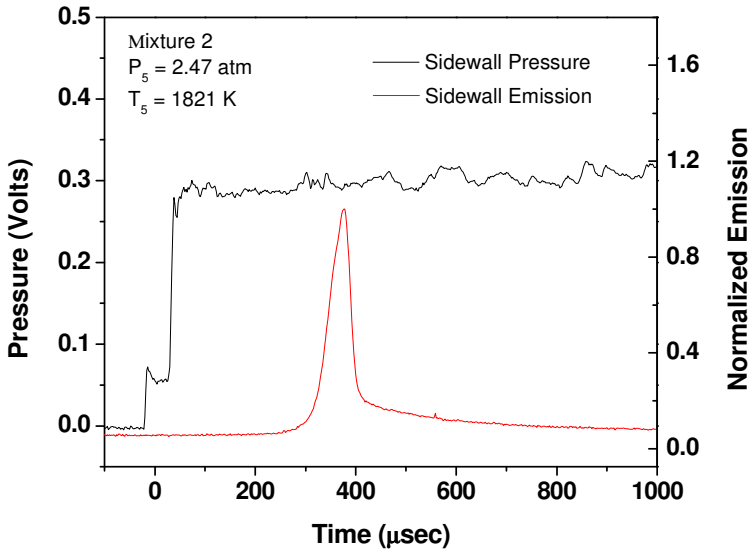

Figure 18. Representative sidewall pressure and emission traces for highly diluted ignition from mixture 2 of this work.

Figure 19 shows representative sidewall pressure and emission traces obtained from mixture 3 in Table 1 for reflected-shock conditions of 2.77 atm and 1424 K. The quality of the traces is good and details are the same as for Figure 18. From looking at

Figs. 17– 19, it can be concluded that the pressure and emission traces recorded are of high quality and can be used to obtain the desired ignition information over a wide range of temperatures and for diluted and non-diluted mixtures.

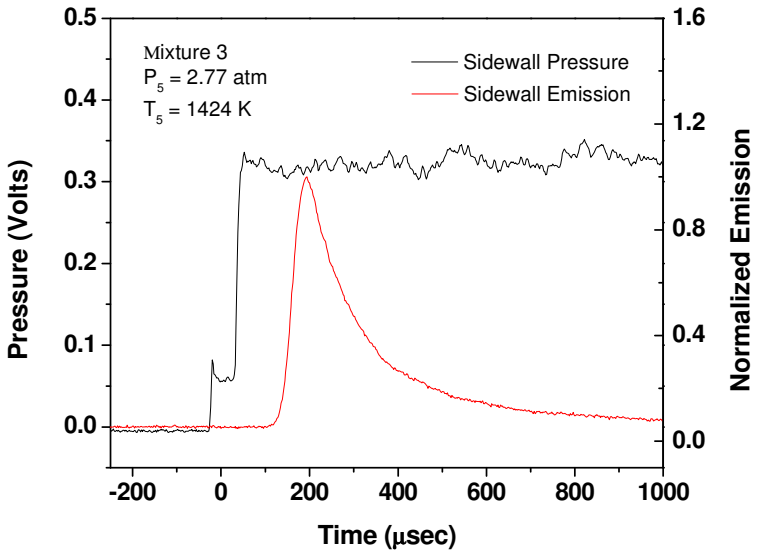

Figure 19. Representative pressure and emission traces for highly diluted ignition from mixture 3 of this work.

Ignition Delay Time Determination

Ignition during reflected-shock conditions is typically determined via two methods: recording chemiluminescence emission from electronically excited radicals such as OH* and CH*, and capturing the rapid pressure increase due to ignition. Normally, both of these measurements are performed at both the sidewall and endwall locations simultaneously. Ideally, the ignition event behind the reflected shock wave starts at the endwall and propagates away from the endwall. Thus, if available, the

pressure measurement at the endwall tends to be the best way to determine ignition delay time. However, it has been shown by Petersen (2009) [8], that in some cases where the ignition event is not energetic enough, there is no measurable rise in pressure that could be identified as the ignition event, so an emission diagnostic needs to be used instead. This absence of a pressure increase at ignition is usually the case when the shock-heated mixture is highly diluted (> 97% by volume) in an inert gas such as Argon or Nitrogen.

Experimental Set-up

As mentioned previously, there are two measurements that need to be done to obtain τ_{ign}: pressure and emission. The locations and instrumentation for the pressure measurements have been described in CHAPTER III. The chemiluminescence measurements at the time of this study were performed only on the sidewall location at 1.6 cm from the endwall. A schematic of the optical set-up utilized to obtain the emission measurements is shown in Figure 20, from Petersen (2009). Note that only the sidewall emission was used for this study.

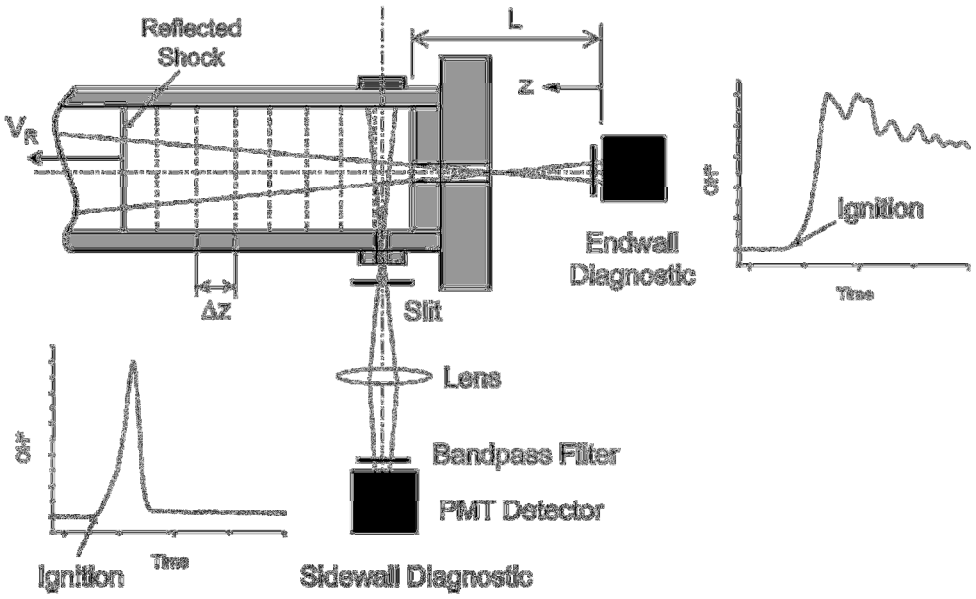

Figure 20. Typical endwall and sidewall emission diagnostics set-up used for chemiluminescence measurements (taken directly from Petersen 2009).

The emission diagnostic set-up consists of a photomultiplier tube (PMT) based on Hamamatsu 1P21 tubes in a homemade housing powered by a Hamamatsu C3830 high-voltage power supply. Included in the housing electronics is the necessary impedance (5-10 kΩ) to allow for a response time on the microsecond-scale. Since the OH* transition of interest is near 307 nm, a bandpass filter centered at 307 nm with a full width at half maximum of 10 nm was used. Additionally, the PMT signal is filtered through a SRS SR560 differential preamplifier.

Measurements with Highly Diluted Mixtures

As mentioned already, mixtures with a high level of dilution (> 97% by volume of an inert diluent) do not produce a significant pressure rise that can be used to

determine the time of ignition. Thus, emission of OH* is the selected method to determine τ_{ign} for the study of mixtures 2 and 3 in Table 1. It is important to mention that for highly diluted mixtures, the emission from the sidewall should be utilized over the endwall emission. The reason for this is that the initial ignition event is influenced by the fact that the detection system sees ignition occurring down the length of the tube rather than just at the endwall region [8]. Using an emission trace, the ignition event is identified by the appearance of the OH* radical. Ignition delay time is then defined as the time between the passage of the reflected shock and the intersection between the steepest slope and the zero-level emission. A schematic showing this definition pictorially is presented in Figure 21.

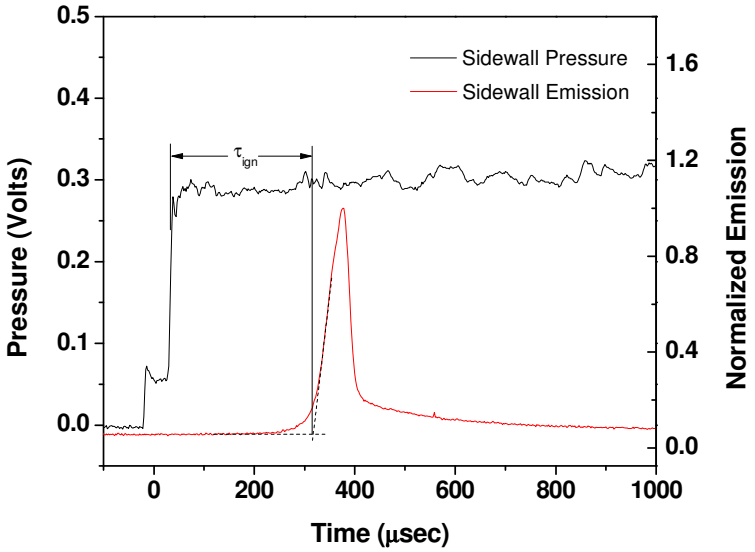

Figure 21. Representative plot for defining ignition delay time for highly diluted mixtures (Mixtures 2 and 3). This particular plot is for mixture 2 in Table 1 at 1821 K and 2.47 atm.

Measurements with Non-Diluted Mixtures

Non-diluted (<90% by volume) mixtures of fuel-oxidizer, on the other hand, exhibit a strong rise in pressure at the time of ignition. It has been determined by Petersen (2009) that when studying non-diluted mixtures, the endwall pressure measurement should be utilized to determine τ_{ign} since ignition starts there and propagates back into the driven section in an ideal scenario. Figure 22 shows a representative pressure measurement used to define τ_{ign} for a non-diluted mixture.

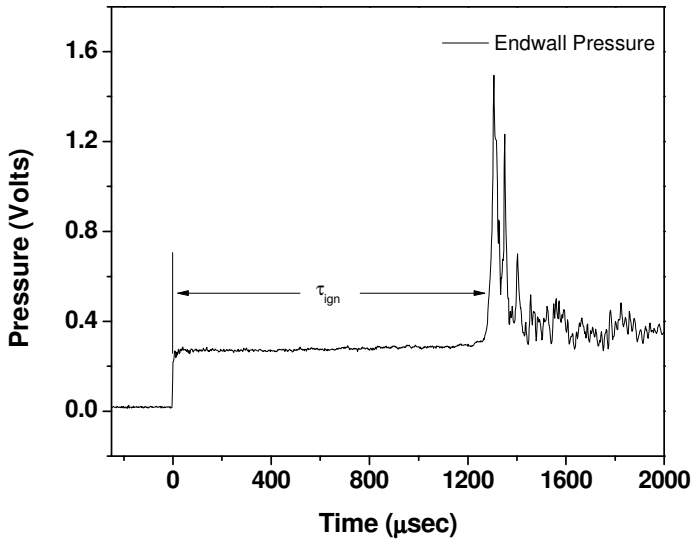

Figure 22. Ignition delay time definition for measurement with non-diluted mixtures that exhibit large energy release. This plot is for mixture 1 in Table 1 at 1498 K and 1.68 atm.

It has also been shown by Petersen (2009) that an endwall emission diagnostic can be used as either a replacement or in addition to the pressure measurement since the ignition time inferred from both diagnostics is identical. Unfortunately, the endwall

diagnostic was not available at the time when the present study was performed, and it was only possible to obtain sidewall emission measurements.

Validation Study Results

Ignition delay time was determined for the mixtures in Table 1 at low pressures (1.3 – 3.3 atm) and for a wide range of temperatures (1000 – 1900 K). To validate the data obtained with the new facility, chemical kinetics modeling for the three mixtures was performed to obtain OH* time histories. The model selected for this study was the AramcoMech 1.0 developed by the Combustion Chemistry Centre at NUI Galway. This model was developed from the bottom up, first with the validation of C_1 hydrocarbon species and, as new data were obtained, it has evolved over the years to include up to C_5-based hydrocarbons. The mechanism has been developed and validated using experimental data from shock-tube experiments, rapid compression machines, flames, jet-stirred and plug-flow reactors. More details on the mechanism can be found at http://c3.nuigalway.ie/mechanisms.html. All the modeling calculations were performed using a constant-volume, homogenous batch reactor simulation from the software Chemkin developed by Reaction Design [9].

The results from the model and the experimental data for all three mixtures are presented in the typical Arrhenius plot of ignition delay time on an inverse temperature axis. Figure 23 shows the comparison of τ_{ign} from the model predictions and the data obtained with the new shock tube for a mixture of undiluted methane-air.

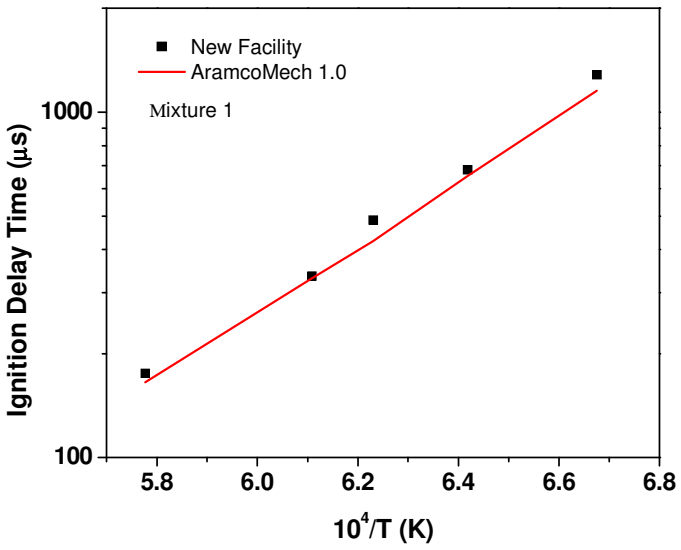

Figure 23. Comparison of experimental and modeled data for mixture 1.

The experimental pressure and temperature were 1.38 – 1.68 atm and 1498 – 1731 K respectively. The data show good agreement between experimental and modeled data and, thus, it can be concluded that measurements for undiluted mixtures using the new facility are validated. Next are the results for highly diluted methane and hydrogen, mixtures 2 and 3 from Table 1. Experimental and modeled data for mixture 2 are shown in Figure 24. Mixture 2 was a stoichiometric methane-oxygen blend diluted in 97.5% Ar. The reflected-shock conditions were 2.46 – 2.72 atm and 1652 – 1930 K. Just as with the undiluted mixture, the experimental data show good agreement with the model. The last mixture was selected because extensive work has been done on the HPST at TAMU, and it is of interest to compare the results between the two facilities. Figure 25 shows a set of experimental and modeled data obtained a couple of years prior to the present thesis with

the original HPST which can be found in [12] and a set of data, model and experiment, obtained with the new facility.

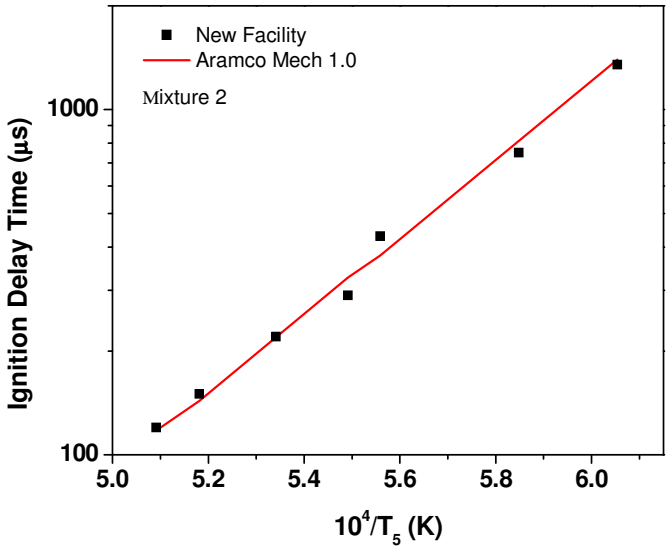

Figure 24. Ignition delay time data from experiments and model for mixture 2.

The experimental conditions on the HPST were 1.4 – 1.9 atm and 1043 – 1739 K, while for the new facility they were 2.7 – 3.3 atm and 1066 – 1550 K. It can be seen from Figure 25 that the experimental data show some discrepancies between experimental ignition times from the HPST and from the new facility; these are attributed to the fact that hydrogen combustion is highly sensitive to pressure and the experimental pressure was different for each facility. However, when comparing each set of data individually with the model predictions, similar level of agreement can be seen from both facilities, where the models capture the overall slope of the data, and it over predicts ignition slightly as the temperature decreases. After looking at the results from the validation study, it can be concluded that the new shock-tube facility replicated the

predictions made by the model. Therefore, this validation study gives the assurance needed to use the new facility to obtain ignition data (or other experiments) for new mixtures.

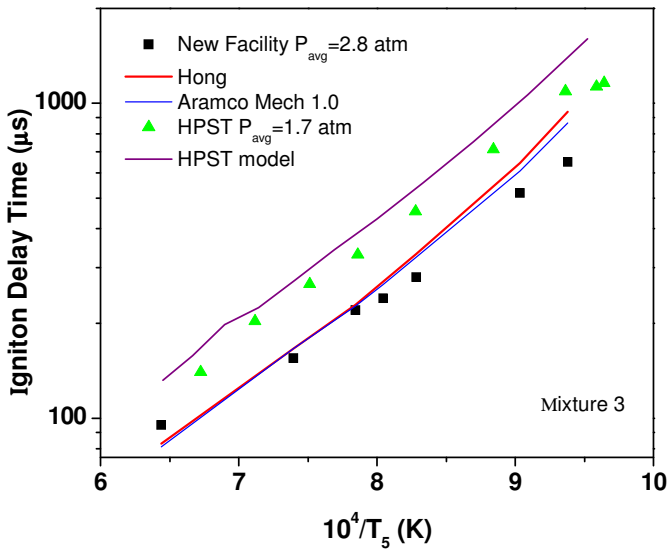

Figure 25. Experimental and modeled data from mixture 3 obtained with the HPST [12] and the new facility.

CHAPTER VI

ACETYLENE STUDY

Acetylene is an intermediate constituent that is formed during the pyrolysis and oxidation of high-order hydrocarbon fuels, and so, it plays an important role in the overall oxidation process [10]. For example, it has been found by several sources that the predominant decomposition products from heavy hydrocarbons include lighter species such as acetylene and ethylene. Thus, to accurately model the combustion of heavy hydrocarbons requires the development of a chemical kinetics mechanism that will be able to predict the oxidation characteristics of acetylene [11].

The Petersen Research Group has been heavily involved in the development/validation of reaction mechanisms with the Combustion Chemistry Centre at the National University of Ireland Galway (NUIG). As mentioned in Chapter IV, the mechanisms developed have been formulated in a hierarchical fashion starting with the simplest hydrocarbons and going up to C_5. Unfortunately, acetylene was a compound that has not been studied yet, and a comprehensive study of its behavior is needed to improve the current model predictions. To support the fact that the model could use some improvement, Figure 26 shows ignition delay time data obtained in a recent study using the original HPST for real fuel-air mixtures of acetylene at equivalence ratios of 0.5, 1 and 2. The model was used to obtain predictions of the ignition delay times of the same mixtures at the reflected-shock conditions. The predictions from the model were obtained using a constant-volume homogenous batch reactor simulation. The

experimental conditions were temperatures from 866 – 1155 K and pressures around 1 atm. It can be seen that the model predicts faster ignition times than the experiments in the high-temperature area (> 1000 K). Something to note as well is that around 1000 K the predictions become slower than experimental data instead of faster, and as the temperature decreases the discrepancies between model and experiments become larger. For example, at an equivalence ratio of 2 and temperature of around 920 K (10.8 in scale on figure 26) the experimental ignition delay time is 626 μsec and the model gives a prediction of 2331 μsec which is almost 4 times larger than the observed ignition delay time.

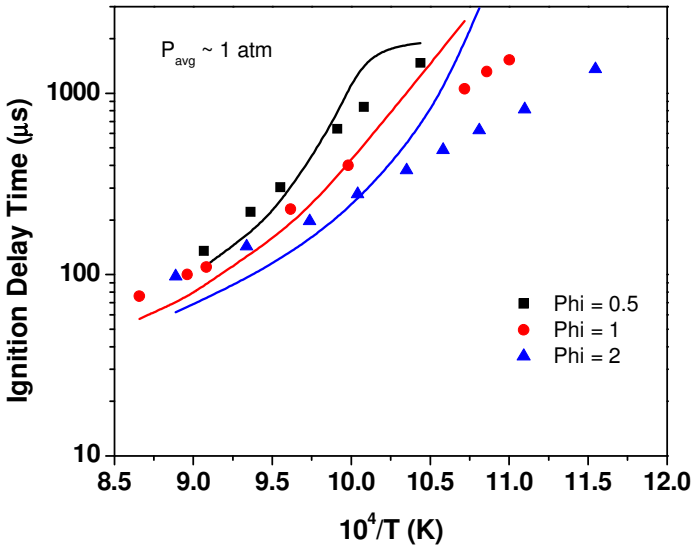

Figure 26. Experimental and modeled ignition data for acetylene-air mixtures at various concentrations taken using the HPST at TAMU.

The full acetylene study on the new shock-tube facility will include highly diluted and undiluted acetylene mixtures for a wide range of temperatures (roughly 900

– 2000 K) and pressures (1 – 10 atm). The results presented in herein, are only for acetylene/O_2 mixtures in 98% Argon. Table 2 presents the composition in percent volume of the mixtures used for this study.

Table 2. Mixture compositions in percent volume for new acetylene data.

Mix	**ϕ**	**% C_2H_2**	**% O_2**	**% Ar**
4	0.5	0.0033	0.0167	0.98
5	1	0.0057	0.0143	0.98
6	2	0.0089	0.0111	0.98

Figure 27 shows representative plots of the pressure and emission profiles for the diluted mixtures in Table 2 at low pressures. As seen for the other mixtures, the pressure profiles have a high signal-to-noise ratio and a relatively small pressure increase that corresponds with the ignition event.

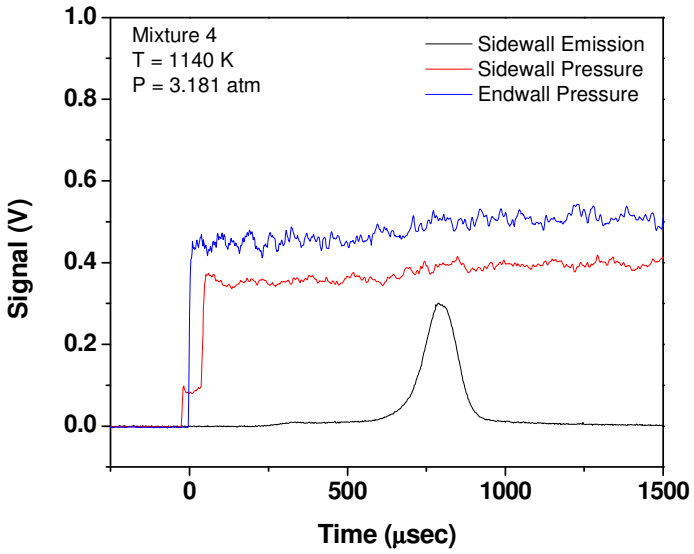

Figure 27. Representative pressure and emission profiles for mixtures 4 and 5.

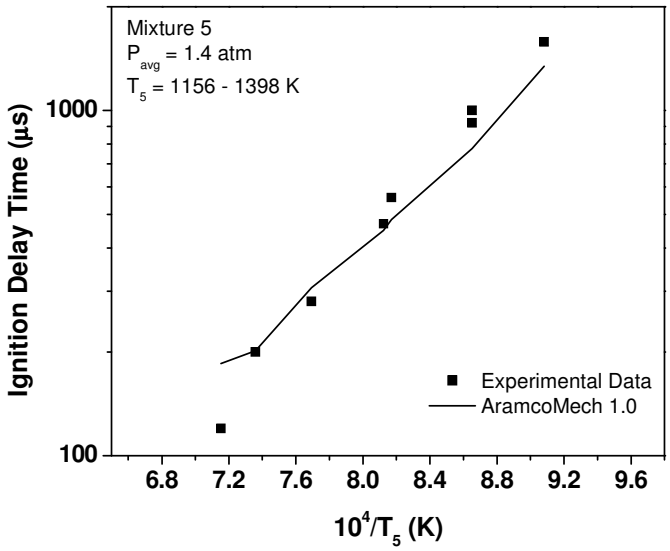

Figure 28. Experimental and modeled ignition delay time for mixture 5.

All the ignition data are shown in a logarithmic plot as a function of inverse temperature. Figure 28 shows the experimental and modeled ignition delay times for mixture 5. For this case, the model does a relatively good job of predicting ignition delay times and capturing the slope of the data over the whole temperature range. An important thing to point out is that while it would seem like the model shows a large discrepancy in the high-temperature data, the ignition delay time is actually closer to the experimental data than the first point (lowest temperature). This apparent discrepancy is due to the fact that the plot is in a log scale and differences seem larger as delay time decreases.

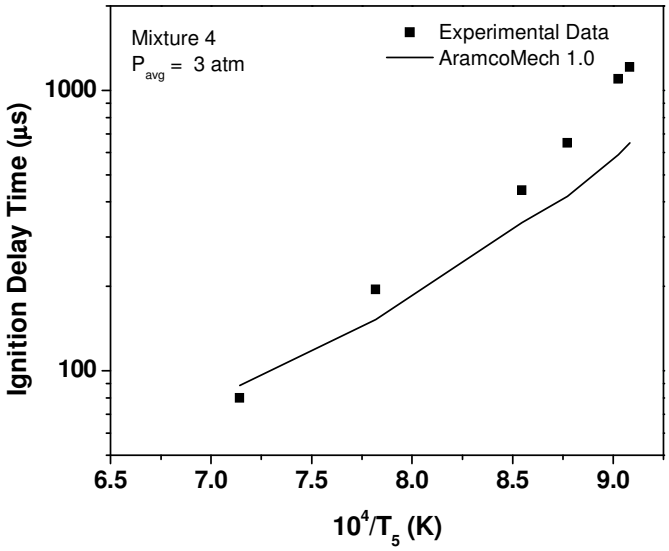

Figure 29. Experimental and modeled ignition delay time for mixtures 4.

The experimental and modeled results for mixture 4 are shown in Figure 29. Experimental and modeled ignition delay time for mixtures 4.. The model does a better job at predicting ignition delay times at high temperature. The slope of the experimental

data is not represented well by the model, and it seems as if the predictions change from too fast to too slow at a temperature close to 1330 K, but more data in the high-temperature region should be taken to verify this behavior. As the temperature decreases, the model predicts much smaller ignition delay times than observed experimentally. For example, at the coldest condition, the model predicts an ignition delay time that is half the experimental value.

The rich mixtures exhibited an interesting behavior in that a double peak on the OH* profile was observed. This type of behavior has been observed before during experiments with heavier hydrocarbons. Figure 30 shows plots of OH* emission versus time for mixture 6 in Table 2 at 1393 K and 2.92 atm, (a) is the experimental profile and (b) is the profile from the kinetics modeling. It is evident from the shape of the profiles that the model does not capture the behavior of acetylene very well. Even though the model does predict more than one peak, it is still inaccurate in regards to the number of peaks, when they appear and the width of the profile. Due to this, it was difficult to assess the best approach to determine ignition delay time from such behavior. Figure 31 shows another example of the experimental (a) and modeled (b) behavior of the rich mixture but now at 1228 K and 3 atm. The double peak behavior is more evident in this case and the model is able to predict it, but, the time of appearance of the second peak, and the width of the profile is very different.

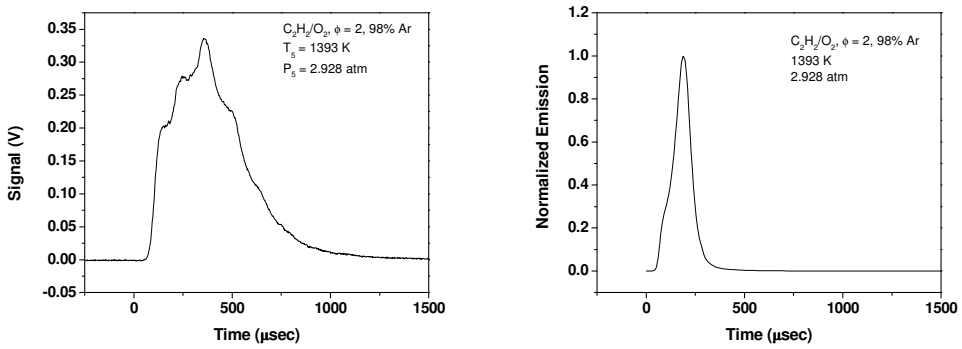

(a) (b)

Figure 30. Experimental (a) and modeled (b) OH* profiles for the rich condition in Table 2 at 1393 K and 2.92 atm.

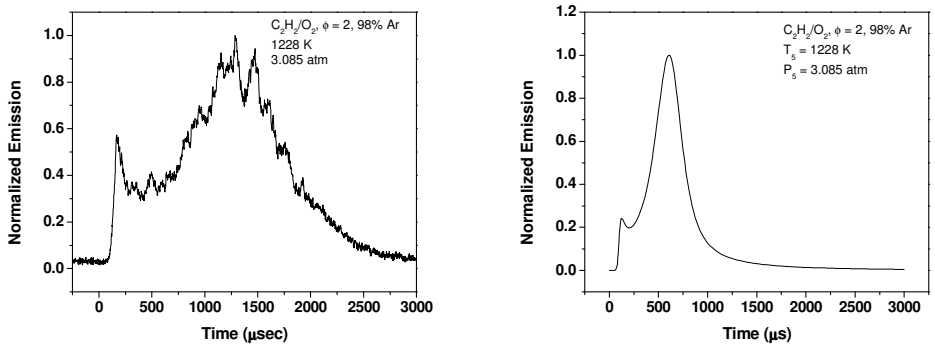

(a) (b)

Figure 31. Experimental (a) and modeled (b) OH* for mixture 6 in Table 2 at 1228 K and 3 atm.

Even though the data presented herein is not the full acetylene study, it can already be seen that the model shows some deficiencies when predicting the behavior of acetylene. This model has been proven to be very accurate for other hydrocarbon species, and it could be even better with the addition of a better kinetics scheme for acetylene combustion characteristics.

CHAPTER VII

RECOMMENDATIONS AND FUTURE WORK

Recommendations

As it was shown previously, the new shock tube is already operational and can be used to obtain accurate data for a variety of experimental conditions. However, there are still some upgrades that are necessary to both obtain additional data and make the operation of the facility more straight forward. First, it is necessary to install a sapphire window on one of the endwall access ports to provide optical access from the endwall point of view. The window on the endwall would provide an additional way to corroborate when the ignition event occurs. Secondly, it would be in the benefit of the experimenter to add the capability of performing experiments remotely if the experimental conditions require it. This could be done by adding an electronic valve on the driver-gas manifold that could be activated from a remote location. Lastly, it would be beneficial to add a master control panel from which all the valves that isolate the vacuum chamber could be controlled. This would not only make the operation of the tube easier but it would also serve as an indicator to show the user which valves are open and closed to avoid exposing delicate equipment such as the turbo-molecular pump to pressures that are too high for it to handle.

Future Work

It is recommended that the ignition delay time data for the full set of acetylene mixtures are obtained. As it was shown in Chapter V, some problems were found when using the experimental emission profiles for OH*. One solution to this anomaly could be using a second chemiluminescence diagnostic with CH* instead and check if the emission traces also present the multiple-feature behavior. Once the ignition delay time measurements are finished, they need to be compared with the predictions from AramcoMech just as it was done in chapter V. As it was shown in Figs. 26 and 28-31, there are currently large discrepancies between the modeled and the experimental results; it is expected to see a similar level of disagreement for the rest of the experimental conditions to be tested. To improve the model, an uncertainty analysis should be performed to find which are the most important reactions (usually 15-20 reactions) and modify their rate constants until there is better agreement between with the measured OH* emission profiles. The features to be matched are typically the time of appearance of OH* and the shape of the overall profile.

Additionally, the facility will be used to apply existing develop new optical diagnostics for emission and absorption measurements as well as for the implementation of techniques to increase the observation time of the facility to more than 15 milliseconds while maintaining steady temperatures and pressures.

REFERENCES

[1] Energy Information Administration, *International Energy Outlook 2013,* *http://www.eia.gov/forecasts/ieo/* accessed on March 2014.

[2] Formin, N.A., "110 Years of Experiments on Shock Tubes," Journal of Engineering Physics and Thermodynamics, **83**, 6, (2010).

[3] Gaydon, A.G., Hurle, J.R., "The Shock Tube in High-Temperature Chemical Physics", 1st Edition, Reinhold Publishing Corporation, New York, 1963.

[4] Payman, W. , Shepherd, W.C., "Explosion Waves and Shock Waves. The Disturbance Produced by Bursting Diaphragms with Compressed Air," Proceedings of the Royal Sociery of London, **186**, 1006, (1946), pp. 293-321.

[5] Petersen. E.L., Rickard M.J.A., Crofton M.W., Abbey E.D., Traum M.J., Kalitan D.M., "A Facility for Gas- and Condensed-Phase Measurements Behind Shock Waves," Meas. Sci. Technol, **16**, 9, (2005) pp. 1716-1729.

[6] Amadio, A.R., Crofton, M.W., and Petersen, E.L., "Test-time extension behind reflected shock waves using CO_2-He and C_3H_8-He driver mixtures," Shock Waves, **16**, pp. 157-165.

[7] Bowman, C.T. and Hanson, R.K., "Shock Tube Measurements of Rate Coefficients of Elementary Gas Reactions," The Journal of Physical Chemistry, **83**, 6, (1979), pp. 757-763.

[8] Petersen, E.L., "Interpreting endwall and sidewall measurements in shock-tube ignition studies," Combust. Sci. Technol., **181**, 9, pp. 1123-1144.

[9] Software CHEMKIN 10112, Reaction Design: San Diego, 2011.

[10] Jachimowski, C. J., "An experimental and analytical study of acetylene and ethylene oxidation behind shock waves," Combustion and Flame, **29**, (1977), pp. 55-66.

[11] Hidaka, Y., Hattori, K., Okuno, T., Inami, K., Abe, T., Koike, T., "Shock-Tube and Modeling Study of Acetylene Pyrolysis and Oxidation," Combustion and Flame, **107**, (1996), pp. 401-417.

[12] A. Kéromnès, W.K. Metcalfe, K.A. Heufer, N. Donohoe, A.K. Das, C.-J. Sung, J. Herzler, C. Naumann, P. Griebel, O. Mathieu, M.C. Krejci, E.L. Petersen,W.J. Pitz, H.J. Curran, Combust. Flame 160 (2013) 995–1011.